Kinetic Mechanism of OMP Synthase: A Slow Physical Step Following Group Transfer Limits Catalytic Rate†

Gary P. Wang,‡ Claus Lundegaard,§ Kaj Frank Jensen,§ and Charles Grubmeyer*,‡

Fels Institute for Cancer Research and Molecular Biology, and Department of Biochemistry, Temple University School of Medicine, 3307 North Broad Street, Philadelphia, Pennsylvania 19140, and Center for Enzyme Research, University of Copenhagen, Sølvgade 83 H DK-1307 Copenhagen K, Denmark

Received August 25, 1998

ABSTRACT: Orotate phosphoribosyltransferase (OMP synthase, EC 2.4.2.10) forms the UMP precursor orotidine 5′-monophophate (OMP) from orotate and α-D-5-phosphoribosyl-1-pyrophosphate (PRPP). Here, equilibrium binding, isotope partitioning, and chemical quench studies were used to determine rate and equilibrium constants for the kinetic mechanism. PRPP bound to two sites per dimer with a K_D of 33 μM. Binding of OMP and orotate also occurred to a single class of two sites per dimer, with K_D values of 3 and 280 μM, respectively. Pyrophosphate binding to two sites was weak with a K_D of 960 μM, and in the presence of bound orotate, its affinity for the first site was enhanced 4-fold (K_D = 230 μM). Preformed E·OMP, E·PRPP, E·PP_i, and E·orotate complexes were trapped as products in isotope partitioning experiments, indicating that each was catalytically competent and confirming a random mechanism. Rapid quench experiments revealed burst kinetics for product formation in both the forward phosphoribosyltransferase and the reverse pyrophosphorolysis reactions. The steady-state rate in the forward reaction was preceded by a burst (n_{fwd} = 1.5/dimer) of at least 300 s^{-1}. In the pyrophosphorolysis reaction, a burst (n_{rev} = 0.7/dimer; $k \geq 300$ s^{-1}) was also noted. These results allowed us to develop a complete kinetic mechanism for OPRTase, in which a rapid phosphoribosyl transfer reaction at equilibrium is followed by a slow step involving release of product. When the microviscosity, η_{rel}, of the reaction medium was increased with sucrose, the forward k_{cat} decreased in proportion to η_{rel} with a slope of 0.8. In the reverse reaction a more limited dependence of k_{cat} (slope = 0.3) was observed. On the basis of the known structures of OPRTase, we propose that a highly conserved, catalytically important, solvent-exposed loop descends during catalysis to shield the active site. In the accompanying paper, the slow product release step is shown to relate to movement of the solvent-exposed loop.

The phosphoribosyltransferases, also designated nucleotide synthases, catalyze the ribose 5-phosphate group transfer required for nucleotide synthesis, and for the formation of the nucleotide-like intermediates for tryptophan and histidine biosynthesis (*1*). The nucleotide synthases constitute two evolutionary families, now designated Types I and II, characterized by distinct folding architectures (*2*). The enzymes are of medical importance. In humans, the OMP[1] synthase reaction serves to activate the prodrug 5-fluorouracil (*3*), and inherited defects in the nucleotide synthases lead to severe inborn disorders of metabolism, including orotic aciduria (*4*), 2,8-dihydroxyadenine lithiasis (*5*), and Lesch-Nyhan syndrome (*6*). The enzymes are also targets for chemotherapies aimed at slowing cell growth, for example, in antiparasitic drugs (*7, 8*).

The kinetics of the Type I enzymes that have been investigated thus far have all been shown to be sequential. In the case of OMP synthase, the mechanism is random (*9*). A functionally ordered mechanism, with PRPP binding first to unliganded enzyme, has been delineated for human (*10*) and schistosomal (*11*) HGPRTases. In the human HGPRTase, on-enzyme phosphoribosyl transfer chemistry is rapid, with a burst of product formation in the forward direction (*10*).

The Type I enzymes proceed through transition states with a high degree of oxocarbenium ion character (*12*). Tao et al. (*13*) used multiple isotope effects to determine the transition-state structure of OMP synthase. In that case, the transition state has an N1-C1′-O(PP_i) axis of 5.65 Å, far longer than the 2.97 Å that represents the sum of the C1−N and C1−O distances in the ground states for OMP and PRPP. Bond orders to incoming base (0.28) and leaving pyrophosphate (essentially 0) are low, leaving a large degree of electron deficiency to be filled by donation from the adjacent ring oxygen. Schramm has documented similar elongated transition states for other enzymatic displacement reactions at the N-nucleosidic bond (*14*−*16*), and they are thought to

* To whom reprint requests should be addressed. Phone: (215) 707-4495. Fax: (215) 707-5529. E-mail: ctg@ariel.fels.temple.edu.

† Supported by NIH grant GM48623 to C.G., and a Center grant from the Danish National Research Foundation to K.F.J.

‡ Temple University School of Medicine.

§ University of Copenhagen.

[1] Abbreviations: EDTA, ethylenediaminetetraacetic acid; GPATase, glutamine phosphoribosylpyrophosphate amidotransferase; HGPRTase, hypoxathine-guanine phosphoribosyltransferase; NMR, nuclear magnetic resonance; OMP, orotidine 5′-monophosphate; OPRTase, orotate phosphoribosyltransferase; PEI, polyethyleneimine; PP_i, inorganic pyrophosphate; PRPP, α-D-5-phosphoribosyl-1-pyrophosphate; PRTase, phosphoribosyltransferase; Tris, tris(hydroxymethyl)aminomethane.

10.1021/bi9820560 CCC: $18.00
Published on Web 12/12/1998

be characteristic of enzymatic glycosyl transfers (*17*). If PRTase reactions occur through oxocarbenium-like transition states, how does the enzyme promote catalysis? In enzymes utilizing pyrimidines, proton removal at the base (N1 pK_a = 9.4 for orotate) may not be required. Similarly, the moderate pK_a of PP_i (9.1; ref *18*) suggests that proton removal at that position may not provide essential catalytic assistance. It has been proposed for GPATase that enzymic assistance in catalysis is provided by strain and proximity effects, with substrate-assisted stabilization of an oxocarbenium ion (*19*).

Crystallographic structures of the Type I nucleotide synthases have revealed a conserved Rossman nucleotide binding fold with a variant "hood" structure that provides for binding and partial solvent occlusion of the base. The most obvious feature of these structures is that the remainder of the active site is relatively solvent-exposed, and that C1′ of bound nucleotide or PRPP, the reactive center, is directly accessible to solvent (*20*, *21*). Clearly, some protein conformational event must occur to generate a solvent-occluded active site. Adjacent to the active site in all known Type I nucleotide synthases is a solvent-exposed peptide loop whose high temperature (b) factors in crystallographic studies indicate conformational flexibility. In several cases these loops have recently been visualized in "down" conformations over the active site. In *Toxoplasma gondii* HGPRTase, an unliganded enzyme form is seen in which this loop is over the active site (*22*). Most convincingly, in GPATase, the loop has been captured in a down position atop an active site occupied by a carbocyclic PRPP analogue (*19*). In that complex, solvent accessibility to the active site is nil.

The biochemistry of the flexible loops is perhaps best known for OMP synthase. It has been shown that residue conservation in the loop (residues 99-RKEAKDHGEGG-109) is higher than in any other region of the primary structure, and some residues of the loop have been shown to be essential (Arg-99 and Lys-103) or important (Lys-100) for catalysis (*23*). It was also demonstrated that Lys-103 is required in the active site formed by the adjacent subunit of the dimer, rather than that formed by its constituent peptide (*24*). In the closely similar *Escherichia coli* OPRTase, crystallization with the weakly inhibitory sulfate anion leads to an asymmetric dimer, with a sulfate anion bound to each active site in the position occupied by the β-phosphorus of PRPP (*25*). One of the loops has been visualized in a down position over the active site of the adjacent subunit. The other loop remains extended into the solvent.

The movement of the flexible loop appears to be integral to catalysis by Type I nucleotide synthases, both to cover the active site and to recruit essential residues to the catalytic locus. We would like to understand the mechanism of that movement and how movement is coupled to substrate binding, group transfer, and product release. In this paper, we present experiments to document the kinetic mechanism of OMP synthase.

EXPERIMENTAL PROCEDURES

Materials. [2-^{14}C] orotic acid was synthesized at Moravek Biochemicals, Inc. (Brea, CA). [γ-^{32}P]ATP was from Amersham. [^{32}P]PP_i was from Dupont NEN Research Products. Thin-layer chromatography plates of polyethyleneimine cellulose were obtained from Alltech (Deerfield, IL). Yeast inorganic pyrophosphatase was purchased from Boehringer-Mannheim Corp. Inorganic chemicals and chromatography solvents were from Fisher. Biochemicals (including OMP) were obtained from Sigma.

Enzyme Preparation. Salmonella typhimurium OPRTase was prepared as described (*23*) and is highly homogeneous. Prior to enzymatic assays, OPRTase stored in 65% saturation $(NH_4)_2SO_4$ at 4 °C was centrifuged and desalted using G-50 gel filtration (*26*). The extinction coefficient ($\epsilon_{280\ nm,\ 1\ mg/mL}$) previously reported for this enzyme, calculated on the basis of the amino acid composition (*27*) was 0.46 (*9*). Quantitative amino acid analysis, performed at the Protein Microchemistry Facility of the Wistar Institute, using procedures described previously (*10*) gave a revised value of 0.51, which is used throughout this study.

Synthesis of Radiolabeled Substrates. [2-^{14}C]OMP was prepared from [2-^{14}C]orotate with the use of OPRTase. [^{14}C]-orotate (10 μCi) was incubated with 10 mM PRPP, 12 mM $MgCl_2$, 1 μg of OPRTase, and 1 μg of yeast inorganic pyrophosphatase in 290 μL of 15 mM NaPi, pH 6.1, at 30 °C for 30 min. The product was purified by ion exchange via high-pressure liquid chromatography (0.4 × 25 cm; ISCO SAX, 5 μm) with isocratic elution at 1 mL/min in 15 mM sodium phosphate, pH 6.1. OMP elutes at 8 min, and orotate elutes at 3.5−5 min. [β-^{32}P]PRPP was prepared from [γ-^{32}P]-ATP using PRPP synthase (a gift of Dr. Robert Switzer) as previously described (*10*). [5-^{32}P]PRPP was prepared enzymatically with the use of ribokinase and PRPP synthase. [^{32}P]-ATP (40 μCi) was incubated with 500 μM ribose, 3 mM $MgCl_2$, and 3 μg of ribokinase in 200 μL of Na-HEPES (*N*-[2-hydroxyethyl]piperazine-*N*′-[2-ethanesulfonate]), pH 7.6, at room temperature for 2 h. Ribokinase was then removed from the reaction mixture using a Centricon-10 apparatus (Amicon) before being used in the subsequent PRPP synthase reaction. The PRPP synthesis mixture contained the enzyme-free ribokinase reaction mixture (~150 μL), 1 mM ATP, 10 mM $MgCl_2$, and 5 μg of PRPP synthase in 600 μL of 50 mM KH_2PO_4 and 50 mM triethanolamine at pH 8.0. The reaction was allowed to proceed at room temperature for 1 h before being applied to a 1 mL column of charcoal/Whatman CF11 cellulose (1:4, w:w) and eluted with 50 mM KH_2PO_4 at pH 8.0. The fractions containing radioactivity were pooled and applied to a Mono-Q column (Pharmacia, 0.5 × 5 cm). The column was eluted at a flow rate of 1 mL/min with a 20 mL linear gradient of 50−500 mM NH_4HCO_3 at pH 8.0. The fractions containing radiolabeled PRPP were detected by Cerenkov radiation, and stored at −20 °C until use.

Steady-State Kinetics Assays. Steady-state initial velocity experiments were conducted by monitoring absorbance changes at 302−304 nm at 30 °C in both the forward phosphoribosyltransferase and the reverse pyrophosphorolysis reactions (*23*). Assay mixtures for the forward reaction contained 75 mM Tris-Cl, 6 mM $MgCl_2$, pH 8.0, and 10−300 μM orotate at 1 mM PRPP, or 20−1000 μM PRPP at 300 μM orotate in a 1.0 mL final volume. For the reverse reaction, assay mixtures were composed of 80 mM Tris-Cl, 3 mM $MgCl_2$, pH 8.0, and 1.5−100 μM OMP at 2 mM PP_i, or 20−2000 μM PP_i at 100 μM OMP in the same final volume. The use of 0.05−0.1 μg of OPRTase provided quantifiable linear initial rates for the calculation of kinetic

parameters. All kinetic data were analyzed using the Cleland program HYPER (*28*), and K_M and V_{max} are reported with their standard errors.

Chemical Quench Experiments. Measurements of reaction kinetics were carried out in an Update Instruments (Madison, WI) Precision Syringe Ram, Model 1010, equipped with a grid-type mixer, largely following the protocols reported for HGPRTase (*10*). For the forward reaction, 80 mM Tris-Cl and 6 mM $MgCl_2$ at pH 8.0 was used as buffer, whereas for the reverse reaction, $MgCl_2$ was reduced to 3 mM. Other reaction components are given in the legends to the tables and figures. Reactions were quenched by ejection through a nozzle into 0.5 mL of 4 M formic acid. The acid-quenched mixtures were centrifuged to remove protein, and chromatographed on PEI cellulose plates in 0.9 M CH_3COOH, 0.3 M LiCl. Under these conditions, the R_f for orotate was 0.6, and that for OMP was 0.2. Radioactive orotate and OMP were quantitated by phosphorimaging (Fuji BAS2000).

Equilibrium Binding. For the binding of PRPP, OMP, orotate, and PP_i, a centrifugal filtration method using Centricon-10 apparatus (Amicon) was employed (*29*). In all cases, 80 mM Tris-Cl in the presence of $MgCl_2$ (3−15 mM, as noted) at pH 8.0 was used as buffer. Other binding mixture components are described in the legends to the figures. To detect the formation of an OPRTase·orotate·PP_i dead end complex, we measured [^{32}P]PP_i binding to OPRTase in the presence of 1.5 mM orotate similarly using centrifugal dialysis. All binding data were subsequently handled using UltraFit (Biosoft) to fit the data to a single-site model. K_D and n values are reported with their standard errors as determined by the fitting progam.

Isotope Partitioning. Isotope partitioning (*30, 31*) experiments were performed at room temperature similarly to those described in Xu et al. (*10*). For isotope partitioning of [β-^{32}P]-PRPP, an equilibrium binding mixture (10 μL) containing 40 μM OPRTase, 40 μM [β-^{32}P]PRPP, and 6 mM $MgCl_2$ in 80 mM Tris-Cl at pH 8.0 was rapidly injected, using a Hamilton syringe, into 800 μL of a rapidly stirred chase solution containing 2.5 mM orotate, 10 mM PRPP, and 15 mM $MgCl_2$ in the same buffer. The reaction was stopped after 2−4 s by the addition of 200 μL of 0.5 M EDTA. Radiolabeled PRPP and PP_i were separated by thin-layer chromatography using PEI cellulose plates (pre-run in water and dried) developed in 0.85 M NaPi at pH 3.4 (*32*), and quantitated with the phosphorimager. Isotope partitioning of [^{32}P]PP_i involved an injection of a 10 μL equilibrium binding mixture containing 450 μM OPRTase, 200 μM [^{32}P]PP_i, and 6 mM $MgCl_2$ in 80 mM Tris-Cl at pH 8.0 into a 2 mL chase solution containing 1 mM OMP, 2 mM PP_i, and 6 mM $MgCl_2$ in the same buffer. The reaction was rapidly quenched after 2 s with 500 μL of 90% formic acid. Radiolabeled PRPP and PP_i were separated and quantitated as described above.

For isotope partitioning of [2-^{14}C]orotate, 10 μL of the equilibrium binding solution containing 150 μM OPRTase, 182 μM [2-^{14}C]orotate, and 6 mM $MgCl_2$ in 80 mM Tris-Cl at pH 8.0 was injected into 800 μL of 1.9 mM orotate, 2 mM PRPP, and 6 mM $MgCl_2$ in the same buffer. The reaction was rapidly quenched with 200 μL of 90% formic acid after 2−4 s. [^{14}C]Orotate and [^{14}C]OMP were separated on PEI cellulose plates in 0.9 M CH_3COOH and 0.3 M LiCl and quantitated with a phosphorimager. Measurements of isotope partitioning of [^{14}C]OMP were performed similarly.

Table 1: Kinetic Parameters for Wild-Type *S. typhimurium* OPRTase at 30 °C

substrate	k_{cat} (s^{-1})	K_M (μM)	k_{cat}/K_M (M^{-1} s^{-1})
Orotate	111 ± 5	18.7 ± 3.4	5.9×10^6
PRPP		18.2 ± 4.5	6.1×10^6
OMP	35 ± 0.5	3.4 ± 0.3	10×10^6
PP_i		30.6 ± 2.5	1.1×10^6

The equilibrium binding solution was prepared using 80 μM OPRTase, 80 μM [^{14}C]OMP, and 3 mM $MgCl_2$ in 80 mM Tris-Cl at pH 8.0. The chase solution contained 4 mM OMP, 100−2000 μM PP_i, 2.5 mM orotate, and 9 mM $MgCl_2$ in the same buffer. The reaction was quenched and analyzed as described above in the isotope partitioning of [^{14}C]orotate. All partitioning experiments were performed on duplicate or triplicate samples in conjunction with controls in which radiolabeled substrates were included only in the chase solution. The amount of radiolabeled ligand bound in the equilibrium binding mixture was calculated on the basis of the K_D and n values obtained from equilibrium binding experiments described above.

Viscosity Studies. Steady-state kinetic experiments in buffers of various viscosities were performed as described above, but with 0−33% (w/v) sucrose included as a microviscogen. The viscosity of the reaction mixtures was determined on triplicate samples at the reaction temperature using an Ostwald viscometer (Fisher) in a thermostated water bath. The viscosity dependencies of steady-state kinetic constants were analyzed (*33*) by plotting $(k_{cat})_o/(k_{cat})$ vs η/η_o, where $(k_{cat})_o$ is the kinetic constant in buffers without the viscogen and η/η_o is the relative viscosity of a solution with respect to the same solution without the viscogen. The slopes of these plots were determined by linear least-squares analysis.

RESULTS

A complete set of macroscopic kinetic constants for the OMP synthase reaction was measured at 30 °C (Table 1). The K_M values in Table 1 are similar, although the k_{cat} values are higher, than values at 30 °C reported earlier (33 and 22 s^{-1} for the forward and reverse reactions, respectively, expressed on a per subunit basis; ref *9*). The k_{cat} values were also determined at 22 °C (50 and 24 s^{-1} for the forward and reverse reactions).

Equilibrium Ligand Binding. Binding measurements for [5-^{32}P]PRPP were made using Centricon ultrafiltration. A Scatchard plot (Figure 1) showed a single class of binding sites. The data were fit to a model with 2 binding sites per dimer, with K_D and n values of 33 ± 5 μM and 1.71 ± 0.08 mol/mol of dimer, respectively.

Binding of OMP also occurred to a single homogeneous class of sites, and gave an n value of 1.63 ± 0.05 mol/mol of dimer and a K_D of 3.1 ± 0.3 μM (Figure 2). Orotate binding was performed using ultrafiltration, and K_D and n values of 283 ± 45 μM and 1.77 ± 0.32 mol/mol of dimer were determined for a single class of sites (Figure 3). Removal of Mg^{2+} from the orotate binding mixtures did not affect K_D or n values.

Binding of [^{32}P]PP_i to OPRTase was detectable but weak. The formation of $MgPP_i$ precipitates above 2 mM precluded studies at high PP_i concentrations. A K_D of 960 μM and an

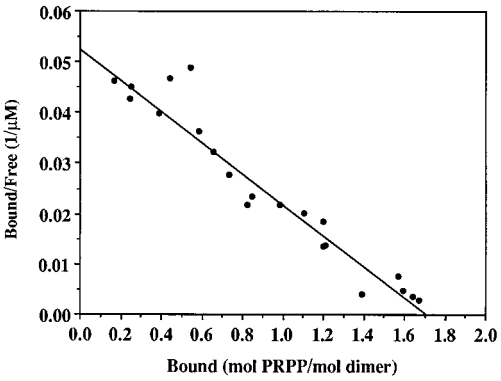

FIGURE 1: Scatchard plot of [5-^{32}P]PRPP binding to OPRTase using Centricon ultrafiltration. The line represents a best fit by nonlinear least-squares regression based on a single-site model according to the following equation: $B = n[L_f/(K_D + L_f)]$, where B represents the number of moles of [5-^{32}P]PRPP bound per mole of OPRTase dimer, n is the total number of binding sites per dimer, and L_f and K_D are the concentration of free [5-^{32}P]PRPP and the dissociation constant for PRPP, respectively. The K_D value that generated the fitted line was 33 μM.

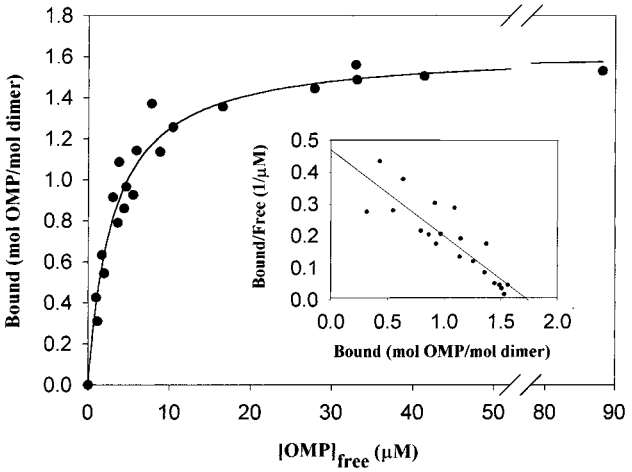

FIGURE 2: Binding of [^{14}C]OMP to OPRTase using Centricon ultrafiltration. The concentrations of [^{14}C]OMP and OPRTase dimer used were 1.4−76 and 1−23 μM, respectively. The curve represents a best fit by nonlinear least-squares regression based on a single-site model according to the following equation: $B = n[L_f/(K_D + L_f)]$, where B represents the number of moles of [^{14}C]OMP bound per mole of OPRTase dimer, n is the total number of binding sites per dimer, and L_f and K_D are the free OMP concentration and the dissociation constant for OMP, respectively. Scatchard analysis of [^{14}C]OMP binding is shown in the inset.

n value of 1.73 were obtained for [^{32}P]PP_i binding to OPRTase (Figure 4; open symbols). Binding of [^{32}P]PP_i was significantly altered by the presence of 1.5 mM orotate. Under these conditions, PP_i bound to a single site per dimer ($n = 1.16$) with a K_D of 230 μM (Figure 4; filled symbols). The existence of additional sites of higher K_D could not be determined.

Phosphoribosyl Group Transfer. Chemical quench experiments (*34*) conducted for the forward reaction showed a rapid burst of [^{14}C]OMP formation, followed by a slower steady-state phase. The steady-state rate (36 s^{-1}) decreased after several turnovers, probably due to build up of inhibitory product OMP. The rate of the burst phase was at least as fast as the resolving time of the instrument (2.5 ms). Figure 5A shows fits to rate constants of 390 and 600 s^{-1} for the burst phase, but faster rates could also be accommodated.

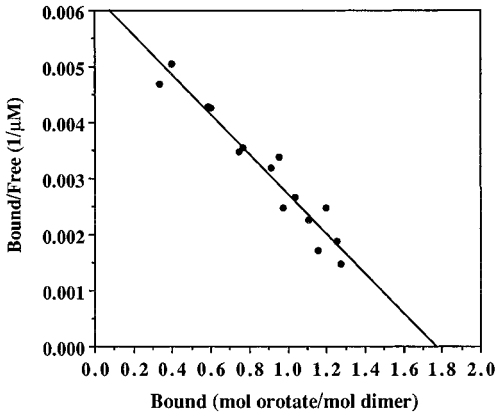

FIGURE 3: Scatchard plot of [^{14}C]orotate binding to OPRTase. Binding of [^{14}C]orotate to OPRTase was conducted at pH 8.0 in the absence of $MgCl_2$ using Centricon ultrafiltration. The concentrations of [^{14}C]orotate and OPRTase employed were 90−1000 μM and 57−210 μM, respectively. The line is a best fit by linear least-squares regression using a single-site model. The K_D and n values were 283 μM and 1.77, respectively.

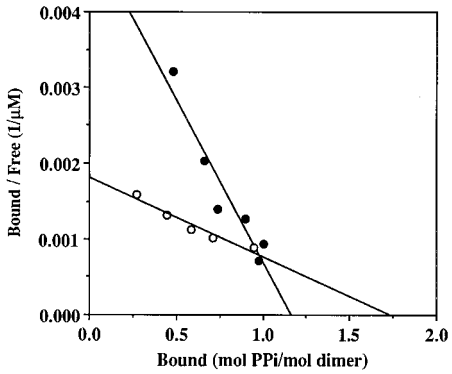

FIGURE 4: Scatchard plots of [^{32}P]PP_i binding to OPRTase. Binding of [^{32}P]PP_i to OPRTase was investigated in the presence (2.5 mM; ●) or absence (○) of orotate using Centricon ultrafiltration. The concentrations of [^{32}P]PP_i and OPRTase employed in the absence of orotate were 100−1200 μM and 206−275 μM, respectively, and in the presence of 2.5 mM orotate, 196−1500 μM and 192−280 μM, respectively. Use of higher [^{32}P]PP_i concentrations was not possible due to the formation of $MgPP_i$ precipitates. Both data sets were fit by linear least-squares regression. In the absence of orotate, the K_D was 960 μM and an n value of 1.73 was extrapolated. In the presence of 2.5 mM orotate, K_D was 230 μM and an n value of 1.16 was extrapolated.

Since the estimation of burst rates of $\geq$300 s^{-1} relies heavily on data obtained from early reaction time (2−4 ms), unambiguous determination of burst rates was not possible from these results. The magnitude of the burst was 1.5 ± 0.1 mol of [^{14}C]OMP/mol of enzyme dimer. Similar results were obtained whether PRPP was preincubated with the enzyme in the first syringe or both substrates were contained in the second syringe. Analogous experiments using 200 μM PRPP yielded results that were similar in both the burst size and burst rate.

In the direction of [^{14}C]OMP pyrophosphorolysis, a burst of [^{14}C]orotate formation was observed, followed by a steady-state phase (Figure 5B). The steady-state rate was 20 s^{-1}, similar to that in spectrophotometric assays at 22 °C. Figure 5B shows fits to burst rates of 390 and 600 s^{-1}, but the data could be accommodated by higher values. The magnitude of the burst was 0.7 ± 0.1 mol of [^{14}C]orotate/mol of enzyme dimer. The values of the burst size for both the forward

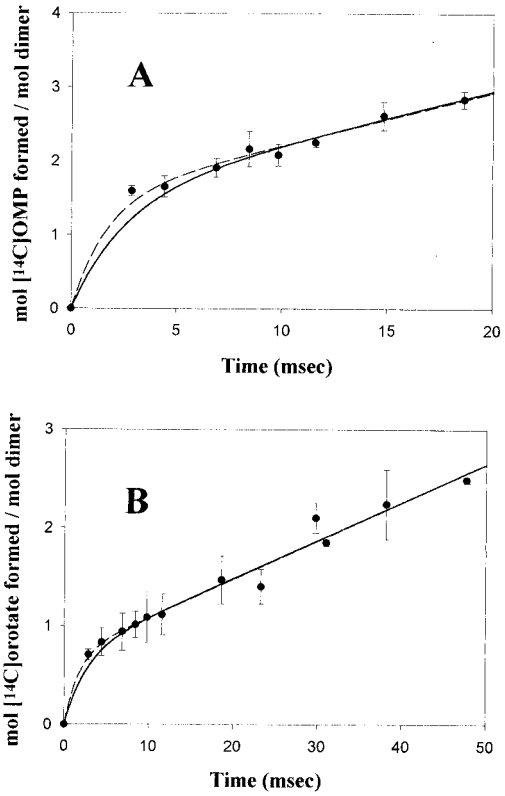

FIGURE 5: Rate of product formation in the (A) forward phosphoribosyltransferase and (B) reverse pyrophosphorolysis reactions. These rapid chemical quench studies were conducted as described in the Experimental Procedures. A burst of product formation followed by a steady-state phase was observed in both reactions, and the burst was faster than the resolving time of the instrument. The data were fit to the equation $y = N(1 - e^{-k_{obs}t}) + kt$ (*34*) using the program SigmaPlot (SPSS, Inc). The burst phase was fit to rates (k_{obs}) of 390 s^{-1} (solid lines; data from 2 to 5 ms were not included in the fit) and 600 s^{-1} (dashed lines; all data points were utilized). The magnitude of the burst (N) was 1.5 mol of [^{14}C]OMP/mol of dimer in the forward reaction and 0.7 mol of [^{14}C]orotate/mol of dimer in the reverse reaction. The steady-state rates, k (36 and 20 s^{-1}, forward and reverse, respectively), were comparable to the values of k_{cat} obtained at 22 °C from spectrophotometric measurements (50 and 24 s^{-1}). Experiments for the forward reaction were performed in triplicate and for the reverse reaction in duplicate. Error bars represent standard errors.

phosphoribosyl transfer and the reverse pyrophosphorolysis reactions were used to calculate a K_{int} (K_5, below) of 2 for on-enzyme catalysis. Rates of on-enzyme group transfer chemstry of 260 and 130 s^{-1} for the forward and reverse chemistry steps, respectively, were calculated (see Disccusion), summing to 390 s^{-1} for the rate of approach to on-enzyme equilibrium.

Isotope Partitioning. Isotope partitioning experiments with [β-^{32}P]PRPP showed that 88% of [β-^{32}P]PRPP calculated to be bound to the enzyme was trapped as [^{32}P]PP_i, when orotate and nonradioactive PRPP were added to start the reaction. When isotope partitioning of orotate was conducted at systematically varied PRPP concentrations (*30*), the maximum amount of bound [^{14}C]orotate trapped as product [^{14}C]-OMP was 55% ± 4%. These results indicate that both the E·PRPP and E·orotate complexes are catalytically competent, consistent with a random mechanism. Since OPRTase also binds orotate in the absence of Mg^{2+} with a similar affinity, an isotope partitioning experiment was performed to test the catalytic competency of metal-free E·orotate complex. The

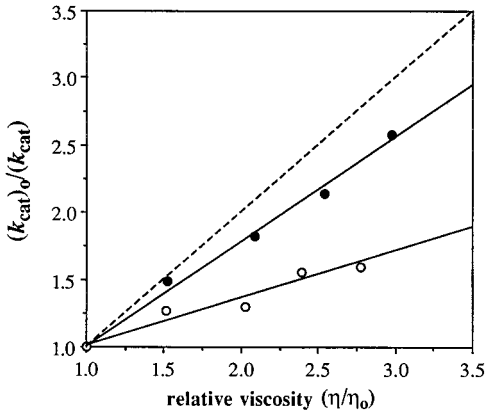

FIGURE 6: Plot of the reciprocal of the relative first-order rate constant $(k_{cat})_o/(k_{cat})$ versus relative viscosity η/η_o for OPRTase in the (●) forward and (○) reverse reaction, using sucrose as a viscogenic agent. Data from steady-state kinetic experiments were analyzed by the program HYPER (*28*) to obtain kinetic parameters. The slope of the linear least-squares line is 0.8 for the forward reaction (●), and 0.3 in the reverse reaction (○). The dashed line has a slope of 1.

results were identical to those performed using Mg^{2+}-containing equilibrium E·orotate binding mixture, indicating that orotate bound to OPRTase in the absence of Mg^{2+} is catalytically competent.

For isotope partitioning of [^{14}C]OMP, variable amounts of PP_i (100−2000 μM) were employed in the chase solution, and the proportion of bound [^{14}C]OMP trapped as [^{14}C]-orotate under these conditions was analyzed using double-reciprocal plots to determine the maximum amount of trapping of E·[^{14}C]OMP, 37% ± 1%. Isotope partitioning experiments with [^{32}P]PP_i showed that 36% of [^{32}P]PP_i calculated to be bound on OPRTase was trapped as [^{32}P]-PRPP, indicating that the E·PP_i complex is also catalytically competent. The catalytic competence of all four E·S complexes firmly established that OPRTase is kinetically random in both the forward phosphoribosyltransferase and the reverse pyrophosphorolysis reactions.

Viscosity Studies. The microviscogen sucrose was used to vary solvent viscosity. When reaction kinetics were measured under different viscosities, k_{cat} for the forward reaction was directly sensitive to viscosity, with a slope of 0.8 (Figure 6; filled symbols). In the reverse reaction, k_{cat} gave a slope of 0.3 (Figure 6; open symbols). These data suggest that a diffusion-limited step contributes to the rate in the forward reaction, whereas the reverse reaction is less limited by diffusion.

DISCUSSION

The key conclusions from our study are that the dimeric *S. typhimurium* OMP synthase proceeds via a random sequential kinetic mechanism in which rapid on-enzyme phosphoribosyl transfer chemistry is followed by a slower product release process. Here we present all of the measured or calculated rate and equilibrium constants for the kinetic mechanism which is diagrammed in Scheme 1 and tabulated in Table 2. Slow product release is shown to be associated with diffusion-controlled processes, which are investigated further in the accompanying paper (*35*).

Random Sequential Mechanism. The 2.6 and 2.3 Å structures of the dimeric *S. typhimurium* OMP synthase in

Table 2: Rate Constants for OPRTase

constant	value	comments
k_1	2.2×10^6 M^{-1} s^{-1}	from K_D(PRPP) and k_{-1}
k_{-1}	71 s^{-1}	NMR PRPP titration
k_2	4.5×10^6 M^{-1} s^{-1}	k_{cat}/K_M(orotate) and [^{14}C]orotate partitioning studies
k_{-2}	117 s^{-1}	[^{32}P]PRPP and [^{14}C]orotate partitioning studies
k_3	$<5 \times 10^6$ M^{-1} s^{-1}	$k_3/k_{-3} = K_3 = 3.6 \times 10^3$ M^{-1}
k_{-3}	<1400 s^{-1}	$k_3/k_{-3} = K_3 = 3.6 \times 10^3$ M^{-1}
k_4	6×10^6 M^{-1} s^{-1}	calculated to fulfill thermodynamic requirement
k_{-4}	20 s^{-1}	[^{32}P]PRPP and [^{14}C]orotate partitioning studies
k_5	260 s^{-1}	chemical quench studies
k_{-5}	130 s^{-1}	chemical quench studies
k_6	79 s^{-1}	[^{32}P]PP$_i$ and [^{14}C]OMP partitioning studies
k_{-6}	7×10^8 M^{-1} s^{-1}	calculated to fulfill thermodynamic requirement
k_7	>200 s^{-1}	see Discussion
k_{-7}	$>2 \times 10^5$ M^{-1} s^{-1}	from K_D(PP$_i$) and k_7
k_8	79 s^{-1}	[^{32}P]PP$_i$ and [^{14}C]OMP partitioning studies
k_{-8}	2.2×10^6 M^{-1} s^{-1}	k_{cat}/K_M(PP$_i$) and [^{32}P]PP$_i$ partitioning studies
k_9	40−120 s^{-1}	[^{14}C]OMP partitioning studies
k_{-9}	$1.3-3.9 \times 10^7$ M^{-1} s^{-1}	from K_D(OMP) and k_9

Scheme 1

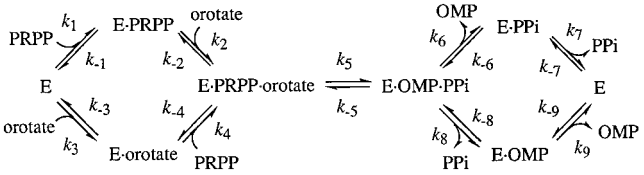

complex with OMP (*20*) and PRPP·orotate (*21*), respectively, display a broad, solvent-exposed active site that is flanked by two important protruding structures, an N-terminal β-hairpin structure known as the "hood" and a solvent-extended loop that appears to be highly flexible. Both active sites occur on one face of the dimer, with the flexible loops occupying a medial position at the dimer interface, and the hood structures lateral to the active sites. In these structures, orotate, or the orotate moiety of OMP, lies under the hood, whereas the pyrophosphate moiety of PRPP is bound adjacent to the flexible loop. Consistent with the random sequential mechanism proposed from steady-state and equilibrium isotope exchanges (*9*), one can envision any of the substrates or products binding directly from solvent. The binding and isotope partitioning results described in this study firmly support the random sequential kinetic mechanism.

A bireactant biproduct enzyme following a random sequential mechanism by definition must show an ability to bind each of its ligands, and its four possible E·S binary complexes are each expected to be catalytically competent. Equilibrium binding experiments clearly indicated that all four ligands were able to bind the apoenzyme. PRPP and OMP bind tightly (33 and 3.1 μM; their K_M values are 18 μM and 3.4 μM, respectively), whereas orotate and PP$_i$ binding were each weak (280 μM and 1 mM; their K_M values are 19 μM and 31 μM, respectively). More conclusive evidence for a functionally random mechanism came from isotope partitioning studies in which trapping of each of the four isotopically labeled enzyme-bound ligands was documented, an indication that the four binary complexes (E·PRPP,
E·orotate, E·OMP, and E·PP$_i$) are each catalytically productive. The partitioning of binary complexes varied with each ligand, and allowed us to determine the dissociation rate constants of ligands from the ternary complexes as discussed in detail below.

Calculation of Rate Constants. A more complete description of the OPRTase kinetic mechanism is a necessary first step toward evaluating the kinetic involvement of the catalytic loop movement during enzymatic turnover as well as determining the exact origin of catalytic lesions resulting from any specific amino acid substitutions. Experiments described here, in conjunction with steady-state measurements and NMR chemical exchange studies detailed in the accompanying paper (*35*), have allowed us to dissect out individual rate constants for a minimal kinetic scheme. The logic of net rate constants, including the net rate expression for a branched release pathway (*36*), was employed throughout the following analysis. Net rate constants relate reversible rate constants and partition coefficients to simplify mathematical consideration of complex kinetic mechanisms. Following Cleland's nomenclature, k' is used to denote the net rate constant for a particular kinetic step. By using measured K_D and k_{cat}/K_M values, together with the isotope partition analysis, we were able to determine the association and dissociation rates for two of the four binary complexes (E·PRPP and E·OMP), and the on-rates for the formation of the two ternary complexes. The relative values of the dissociation rates for each of the four ligands from the ternary complexes were also determined. The minimal values for these constants and for the rates of phosphoribosyl transfer chemistry were then determined from the known value of K_5 by simultaneous solution of kinetic equations. Finally, the use of measured K_D and k_{cat} values yielded the association and dissociation rates for the remaining two binary complexes (E·orotate and E·PP$_i$).

The dissociation rate constant for PRPP, k_{-1} (71 s^{-1}), was measured by PRPP titration using ^{1}H and ^{31}P NMR, as discussed in detail in the accompanying paper (*35*). The association rate constant k_1 (2.2×10^6 M^{-1} s^{-1}) was then calculated from K_D for PRPP (33 μM) and k_{-1}. The association rate constant for orotate binding to E·PRPP, k_2 (4.5×10^6 M^{-1} s^{-1}), was determined from the measured k_{cat}/K_M for orotate (2.5×10^6 M^{-1} s^{-1}), and its forward partition coefficient ($P_{c(orotate)} = k'_5/(k'_5 + k_{-2})$). Isotope partitioning of the E·[^{14}C]orotate binary complex allowed direct measurement of $P_{c(orotate)}$ (0.55) and thus k_2.

$$k_2 = [k_{cat}/K_{M(orotate)}]/P_{c(orotate)}$$

The dissociation rate constants of orotate (k_{-2}) and of PRPP (k_{-4}) from the reactive ternary complex E·PRPP·orotate were not directly measured, but their relative ratios (k_{-2} : k_{-4} = 6:1) were determined by relating isotope partitioning results using preformed binary complexes E·[^{32}P]PRPP ($P_{c(PRPP)}$ = 0.88) and E·[^{14}C]orotate ($P_{c(orotate)}$ = 0.55) according to the following relationships:

$$P_{c(PRPP)} = k'_5/(k'_5 + k_{-4})$$

$$P_{c(orotate)} = k'_5/(k'_5 + k_{-2})$$

$$\frac{k_{-2}}{k_{-4}} = \frac{P_{c(PRPP)}(1 - P_{c(orotate)})}{P_{c(orotate)}(1 - P_{c(PRPP)})}$$

From these relative rates, we were able to calculate the values of these dissociation rate constants (see below).

By using the relationships of rate and dissociation constants for the theromodynamic box describing the formation of the E·PRPP·orotate ternary complex from E ($K_1K_2 = K_3K_4$), we calculated the association rate constant of PRPP binding to E·orotate, k_4 (6×10^6 M^{-1} s^{-1}), according to the following equation:

$$k_4 = [K_{D(orotate)}k_2k_{-4}]/[K_{D(PRPP)}k_{-2}]$$

The value of k_4 is in good agreement with the k_{cat}/K_M value for PRPP of 6×10^6 M^{-1} s^{-1} determined at 30 °C (Table 1).

Following the logic of Rose (*30*), the dissociation and association rate constants of the binary E·OMP complex (k_9 and k_{-9}) were placed within limiting values (40−120 s^{-1} and 1.3−3.9 $\times$ 10^7 M^{-1} s^{-1}, respectively) by using the isotope partitioning approach and K_9. To derive the dissociation and association rate constants of OMP (k_6 and k_{-6}) and PP_i (k_8 and k_{-8}) from the reactive ternary product complex E·OMP·PP_i, we employed the same strategy as outlined above for the E·PRPP·orotate substrate complex. The steady-state kinetic parameter k_{cat}/K_M for PP_i (8.0×10^5 M^{-1} s^{-1}) in conjunction with isotope partitioning of E·[^{32}P]PP_i binary complexes ($P_{c(PP_i)} = k'_{-5}/(k'_{-5} + k_8)$ = 0.36) allowed calculation of an on-rate (k_{-8}) of 2.2×10^6 M^{-1} s^{-1} for PP_i binding to E·OMP.

$$k_{-8} = [k_{cat}/K_{M(PP_i)}]/P_{c(PP_i)}$$

The observation that approximately equal proportions of E·[^{14}C]OMP and E·[^{32}P]PP_i binary complexes (37% and 36%, respectively) were successfully trapped as radiolabeled products indicates that the values of dissociation rate constants of OMP (k_6) and PP_i (k_8) from the ternary product complex E·OMP·PP_i are comparable (k_6:k_8 = 1:1), on the basis of the following relationship:

$$P_{c(OMP)} = k'_{-5}/(k'_{-5} + k_6) = 0.37$$

$$P_{c(PP_i)} = k'_{-5}/(k'_{-5} + k_8) = 0.36$$

$$k_6/k_8 = [P_{c(PP_i)}(1 - P_{c(OMP)})]/[P_{c(OMP)}(1 - P_{c(PP_i)})]$$

This rate relationship was then utilized to obtain the values of the dissociation rate constants (see below).

Finally, the value of k_{-6} (7×10^8 M^{-1} s^{-1}), the association rate constant for OMP binding to E·PP_i, was calculated to balance the equilibrium binding within the closed system (steps describing the formation of the E·OMP·PP_i ternary complex from E, or $K_6K_7 = K_8K_9$) according to the following equation:

$$k_{-6} = [K_{D(PP_i)}k_6k_{-8}]/[K_{D(OMP)}k_8]$$

Thus far, we have determined the association and dissociation rate constants for the E·PRPP and E·OMP complexes (k_1, k_{-1}, k_{-9}, k_9) and the on-rates for formation of the two ternary complexes (k_2, k_4, k_{-6}, k_{-8}). By using the known value of 2 for K_5 (k_5/k_{-5}), the known partition coefficients for the four enzyme·substrate binary complexes, and the relative ratios of the dissociation rate constants from the two ternary complexes (k_{-2}/k_{-4} and k_6/k_8), we obtained the *minimal* values for the individual dissociation rate constants of ligands from the reactive ternary complexes (k_{-2}, k_{-4}, k_6, k_8) and for the rates of on-enzyme phosphoribosyl transfer chemistry (k_5 and k_{-5}) (Table 2) that were consistent with the k_{cat} values. Higher values for these rate constants could also be accommodated by our data. Unambiguous determination of their absolute values, however, was not possible on the basis of our results.

By using the values of 50 and 24 s^{-1} for the forward and reverse k_{cat} in the following equations for a branched release mechanism (*36*), we calculated the dissociation rate constants for orotate (k_{-3}) and PP_i (k_7). From these values and the measured K_D, the association rate constants (k_3 and k_{-7}) were obtained.

$$k'_5 = k_5(k_6 + k_8)/(k_6 + k_8 + k_{-5})$$

$$k'_{-5} = k_{-5}(k_{-2} + k_{-4})/(k_{-2} + k_{-4} + k_5)$$

$$1/k_{cat(forward)} = 1/k'_5 + 1/[(k_6 + k_8)/(1 + k_6/k_7 + k_8/k_9)]$$

$$\frac{1}{k_{cat(reverse)}} = \frac{1}{k'_{-5}} + \frac{1}{(k_{-2} + k_{-4})/(1 + k_{-2}/k_{-1} + k_{-4}/k_{-3})}$$

The random sequential mechanism and rate constants of Scheme 1 and Table 2 provide excellent agreement with the available data, including all equilibrium binding, isotope partitioning, chemical quench, and steady-state kinetic studies (*9*, *23*). Pre-steady-state simulations using Kinsim (*37*) predict burst kinetics for both the forward and reverse reactions with burst sizes similar to those observed in chemical quench experiments. The overall equilibrium constant K_{eq} calculated on the basis of the derived rate constants in Table 2 is 0.3, which is in good agreement with the measured K_{eq} value of 0.1 reported by Bhatia et al. (*9*). Values of K_{eq} for the OPRTase reaction ranging from 0.07 to 0.7 have been reported (see ref *9*). The variations of Mg^{2+} concentrations used in our study may account for the minor difference in K_{eq} values.

In a random mechanism, two routes are available for substrate binding and product release in each direction. With OPRTase, PRPP and OMP binding occurs rapidly from moderate concentrations. In the forward direction, OMP and PP_i leave the enzyme ternary complex with nearly equal rates, whereas, in the reverse reaction, orotate will dissociate first

about 85% of the time. For the minor pathway in which PRPP dissociates first from the E·PRPP·orotate ternary complex, we can only place broad limits on the association and dissociation rates for the E·orotate binary complex (k_3 and k_{-3}, respectively). One feature of some steady-state random bireactant mechanisms is nonhyperbolic v/[S] plots at intermediate concentrations of the fixed substrates (*38*). However, such behavior is only observed when there is a kinetically preferred binding route (i.e., the two available binding routes differ by more than 10-fold in their rates). Such nonhyperbolic v/[S] curves have not been reported for OPRTase, although rigorous analyses have not been conducted to detect this behavior.

Rapid Phosphoribosyl Transfer Chemistry. Rapid on-enzyme phosphoribosyl transfer chemistry with slow product release has previously been reported for two nucleotide synthases, human HGPRTase (*10*), which like OPRTase follows Type I PRTase architecture, and *S. typhimurium* NAPRTase (*39*), which is likely to be a second example of a Type II PRTase (*2*). In HGPRTase, the forward phosphoribosyl transfer rate (131 s^{-1}) is 22-fold more rapid than the overall rate of forward catalysis (6.0 s^{-1}). The group transfer rate of at least 500 s^{-1} in NAPRTase is also far greater than the forward k_{cat} (2.3 s^{-1}). Rapid chemistry was expected for OPRTase on the basis of equilibrium isotope exchange studies (*9*). The chemical quench experiments in this study demonstrate that OPRTase undergoes rapid on-enzyme phosphoribosyl group transfer followed by slow product release. The burst rates in both the forward phosphoribosyl transfer and the reverse pyrophosphorolysis reactions were faster than the resolving time of our rapid quench instrument, and were consistent with a rate of approach to on-enzyme equilibrium of $\geq$300 s^{-1}. The amplitude of the burst was 1.5 mol of [^{14}C]OMP/mol of dimer in the forward direction and 0.7 mol of [^{14}C]orotate/mol of dimer in the reverse, thus summing to about 2 per dimer. The simplest interpretation consistent with these data is that rapid chemistry allows the establishment of an equilibrium between the substrate and product ternary complexes. The on-enzyme equilibrium (K_{int}, or K_5, Scheme 1) is 2, favoring the E·OMP·PP_i ternary complex over E·PRPP·orotate.

Product Inhibition. The association rate constant of 7×10^8 M^{-1} s^{-1} for OMP binding to E·PP_i (k_{-6}) approaches the diffusion-controlled limit for a bimolecular process (*40*). The magnitude of k_{-6} predicts that even small amounts of product OMP generated by the forward reaction will be inhibitory. In fact, a pronounced rate decrease is observed early in the steady-state phase. A full time course simulation by Kinsim (ref *37*; simulation not shown) using rate constants derived in this study also predicts strong product inhibition. Product inhibition of OPRTase was first noted by Lieberman et al. (*41*), who observed that this inhibition could be partially removed using OMP decarboxylase.

Viscosity Studies. Experimental manipulation of microviscosity has been used to detect and quantitate diffusion-limited steps in an overall reaction scheme (*33*, *42*). A kinetic step that involves on-enzyme chemical interconversion is expected to show viscosity independence. In contrast, product release could show viscosity dependence if it is associated with diffusion-controlled processes. In both the forward and the reverse OPRTase reactions, steady-state kinetic experiments in buffers of various viscosities show viscosity dependence of the first-order rate constant k_{cat}. In the forward phosphoribosyltransferase reaction, k_{cat} is highly viscosity-dependent (80%), indicating that, at saturating substrate concentrations, a diffusion-controlled step is predominantly rate-limiting. Since product release is slow relative to the chemistry step, the diffusion-controlled process detected by viscosity is likely to be associated with product release. Experiments for the pyrophosphorolysis reaction show a more limited viscosity dependence of k_{cat} (30%). As the chemistry step is not expected to be viscosity-sensitive, the diffusion-controlled process is also associated with product release. We have attributed this diffusion-controlled process to the opening of the catalytic flexible loop accompanying PRPP release and have measured the rates of loop opening/closing using ^{1}H and ^{31}P NMR spectroscopy (*35*).

ACKNOWLEDGMENT

Gary Wang was supported through the M.D./Ph.D. program of Temple University School of Medicine. We thank Dr. David Speicher, Wistar Institute, for quantitative amino acid analysis.

REFERENCES

1. Musick, D. L. (1981) *CRC Crit. Rev. Biochem. 11*, 1−34.
2. Eads, J. C., Ozturk, D., Grubmeyer, C., and Sacchettini, J. C. (1997) *Structure 5*, 47−58.
3. Chu, E., and Takimoto, C. H. (1993) in *Cancer: Principles & Practice of Oncology* (DeVita, V. T., Jr., Hellman, S., and Rosenberg, S. A., Eds.) 4th ed., Vol. 1, pp 362−365, Lippincott, Philadelphia, PA.
4. Suttle, J. P., Becroft, D. M. O., and Webster, D. R. (1989) in *The Metabolic Basis of Inherited Disease* (Scriver, C. R., Beaudet, A. L., Sly, W. S., and Valle, D., Eds.) 6th ed., pp 1095−1126, McGraw-Hill, New York.
5. Simmonds, H. A., Sahota, A. S., and van Acker, K. J. (1989) in *The Metabolic Basis of Inherited Disease* (Scriver, C. R., Beaudet, A. L., Sly, W. S., and Valle, D., Eds.) 6th ed., pp 1029−1044, McGraw-Hill, New York.
6. Stout, J. T., and Caskey, C. T. (1989) in *The Metabolic Basis of Inherited Disease* (Scriver, C. R., Beaudet, A. L., Sly, W. S., and Valle, D., Eds.) 6th ed., pp 1007−1028, McGraw-Hill, New York.
7. Ullman, B., and Cater, D. (1995) *Infect. Agents Dis. 4*, 29−40.
8. Kanaani, J., Maltby, D., Somoza, J. R., and Wang, C. C. (1997) *Eur. J. Biochem. 244*, 810−817.
9. Bhatia, M. B., Vinitsky, A., and Grubmeyer, C. (1990) *Biochemistry 29*, 10480−10487.
10. Xu, Y., Eads, J. C., Sacchettini, J. C., and Grubmeyer, C. (1997) *Biochemistry 36*, 3700−3712.
11. Yuan, L., Craig, S. P., III, McKerrow, J. H., and Wang, C. C. (1992) *Biochemistry 31*, 806−810.
12. Goitein, R. K., Chelsky, D., and Parsons, S. M. (1978) *J. Biol. Chem. 253*, 2963−2971.
13. Tao, W., Grubmeyer, C., and Blanchard, J. S. (1996) *Biochemistry 35*, 14−21.
14. Parkin, D. W., and Schramm, V. L. (1987) *Biochemistry 26*, 913−920.
15. Horenstein, B. A., Parkin, D. W., Estupinan, B., and Schramm, V. L. (1991) *Biochemistry 30*, 10788−10799.
16. Kline, P. C., and Schramm, V. L. (1995) *Biochemistry 34*, 1153−1162.
17. Matsui, H., Blanchard, J. S., Brewer, C. F., and Hehre, E. J. (1989) *J. Biol. Chem. 264*, 8714−8716.
18. Dawson, R. M. C., Elliott, D. C., Elliott, W. H., and Jones, K. M. (1986) *Data for Biochemical Research*, 3rd ed., Oxford Science Publications, Oxford, U.K.
19. Krahn, J. M., Kim, J. H., Burns, M. R., Parry, R. J., Zalkin, H., and Smith, J. L. (1997) *Biochemistry 36*, 11061−11068.

20. Scapin, G., Grubmeyer, C., and Sacchettini, J. C. (1994) *Biochemistry 33*, 1287−1294.
21. Scapin, G., Ozturk, D. H., Grubmeyer, C., and Sacchettini, J. C. (1995) *Biochemistry 34*, 10744−10754.
22. Schumacher, M. A., Carter, D., Roos, D. S., Ullman, B., and Brennan, R. G. (1996) *Nat. Struct. Biol. 3*, 881−887.
23. Ozturk, D. H., Dorfman, R. H., Scapin, G., Sacchettini, J. C., and Grubmeyer, C. (1995) *Biochemistry 34*, 10755−10763.
24. Ozturk, D. H., Dorfman, R. H., Scapin, G., Sacchettini, J. C., and Grubmeyer, C. (1995) *Biochemistry 34*, 10764−10770.
25. Henriksen, A., Aghajari, N., Jensen, K. F., and Gajhede, M. (1996) *Biochemistry 35*, 3803−3809.
26. Penefsky, H. S. (1977) *J. Biol. Chem. 252*, 2891−2899.
27. Gill, S. T., and von Hippel, P. H. (1989) *Anal. Biochem. 182*, 319−326.
28. Cleland, W. W. (1979) *Methods Enzymol. 63*, 103−139.
29. Stitt, B. L. (1988) *J. Biol. Chem. 263*, 11130−11137.
30. Rose, I. A. (1980) *Methods Enzymol. 64*, 47−59.
31. Rose, I. A. (1995) *Methods Enzymol. 249*, 315−340.
32. Jensen, K. F., Houlberg, U., and Nygaard, P. (1979) *Anal. Biochem. 98*, 254−263.
33. Hardy, L. W., and Kirsch, J. F. (1984) *Biochemistry 23*, 1275−1282.
34. Johnson, K. A. (1995) *Methods Enzymol. 249*, 38−61.
35. Wang, G. P., Cahill, S. M., Liu, X., Girvin, M. E., and Grubmeyer, C. (1999) *Biochemistry 38*, 284−295.
36. Cleland, W. W. (1975) *Biochemistry 14*, 3220−3224.
37. Barshop, B. A., Wrenn, R. F., and Frieden, C. (1983) *Anal. Biochem. 130*, 134−145.
38. Segel, I. H. (1975) *Enzyme Kinetics*, John Wiley & Sons, New York.
39. Gross, J. W., Rajavel, M., and Grubmeyer, C. (1998) *Biochemistry 37*, 4189−4199.
40. Fersht, A. R. (1985) *Enzyme Structure and Mechanism*, 2nd ed., W. H. Freeman, New York.
41. Lieberman, I., Kornberg, A., and Simms, E. S. (1955) *J. Biol. Chem. 215*, 403−415.
42. Bazelyansky, M., Robey, E., and Kirsch, J. F. (1986) *Biochemistry 25*, 125−130.

BI9820560